journal

J. Am. Ceram. Soc., 80 [1] 27–36 (1997)

Microstructure Development in Al_2O_3-Platelet-Reinforced Ce-ZrO_2/Al_2O_3 Composites

Ryan K. Roeder,* Kevin P. Trumble,* and Keith J. Bowman*

School of Materials Engineering, Purdue University, West Lafayette, Indiana 47907

Composites containing Ce-ZrO_2, Al_2O_3, and aligned Al_2O_3 platelets were produced by centrifugal consolidation and pressureless sintering, followed by beat treatments at 1600°C for varied duration. Constituents in the consolidated microstructures were either uniformly distributed throughout or segregated into gradient layers, depending critically on platelet content. Quantitative image analysis was used to examine microstructure development with heat treatment. Changes in the volume fraction, dimensional anisotropy, and gradient of pores and platelets, as well as changes in the phase gradient, were quantified. Microstructure development was strongly dependent on the initial microstructure design attained trom suspension processing.

I. Introduction

EFFORTS to produce ceramic matrix composites (CMCs) for high-temperature structural applications have focused on the superior properties of fiber-reinforced CMCs. However, fiber-reinforced CMCs are currently limited by cost. impractical processing methods. and property degradation at high temperatures. Despite sacrifices in some properties. platelet-reinforced CMCs may offer a more feasible, near-term solution for producing CMCs usable in high-temperature structural applications.

In platelet-containing composites, many researchers have examined microstructure-property relationships' [8] and processing–microstructure relationships;[5–10] however, microstructure development during heat treatment has received little attention."' [12] Microstructure development in platelet composites is governed by many factors, including the size. shape, orientation, location, and interaction of the reinforcement phase and matrix phases. With scientific understanding and quantitative results for microstructure development. sintering and annealing treatments could be used to tailor a microstructure to achieve optimized properties. Furthermore, examination of microstructure development may facilitate design ofmicrostructures more amenable to tailoring by heat treatment.

Platelets can be incorporated in composites by a variety of processing approaches: however, optimal approaches can be manipulated to control both orientation and microstructurnl design for property optimization. Consolidation methods consistent with microstructure control favor suspension routes that achieve high packing densities via platelet alignment. Factors critical to efficient packing of aligned platelets include repulsive interparticle forces and high settling forces on particles. Centrifugal consolidation uniquely and practically produces highly controlled microstructures, through control of the centrifugal forces on particles, constituent particle size, particle size distribution, constituent density. relative constituent amounts, suspension viscosity, and interparticle forces. Centrifugal consolidation and pressure filtration have been used to produce more consistent and dense cakes than is generally possible by other consolidation techniques." [19] The efficacy of centrifugal consolidation for aligning anisometric particles has also been demonstrated."'"

The Ce–ZrO_2/Al_2O_3/Al_2O_3-platelet system provides the additional benefit of transformation toughening to a platelet-reinforced microstructure. Introducing large, nontransforming microstructural units (e.g., Al_2O_3 layers) into Ce–ZrO_2 has been shown to widen an otherwise elongated transformation zone ahead of the crack tip." Nontransforming Al_2O_3 layers force adjacent widening of the transformation zone. Increasing crack tip shielding. This anisotropic microstructure makes possible large increases in fracture toughness (in Ce–ZrO_2, from ~5 to 17.5 MPa·$m^{1/2}$).[22] The presence of Al_2O_3 platelets might induce further transformation zone widening. and the platelets could lead to coincident toughening by platelet pullout, crack deflection, crack bridging. and modulus load transfer.

A novel centrifugal processing approach has been developed to produce multicomponent, multilayered composites with controllable microstructures." [20] In prior processing of multilayered ceramic composites by suspension consolidation, investigators have focused on consolidating separate suspensions into alternating" or sequential" homogeneous layers. These efforts have focused on preventing size and mass segregation in multicomponent suspensions (methods of preventing segregtion are discussed in Ref. 20), most often by utilizing attractive interparticle forces or high solids contents. Contrary to these and other prior efforts, segregation can be exploited rather than avoided. By applying large settling forces on particles, centrifugal consolidation can be used to segregate dispersed, multicomponent suspensions into gradient layers, given proper consideration for constituent size and density." [20] The resulting microstructures are unique, containing continuous phase and size gradients within each layer. Composites containing multiple gradient layers are termed functionally gradient laminates (FGLs).

In this study. quantitative image analysis is used to examine microstructure development in centrifugally consolidated composites containing Ce–ZrO_2, Al_2O_3, and aligned Al_2O_3 platelets. The composite constituents are either uniformly distributed throughout or segregated into gradient layers, depending critically on the platelet content."' Quantitative image analysis is used to analyze pore, platelet, and phase gradient evolution with heat treatment. paying special attention to the influence of the green microstructure design on microstructure development during heat treatment.

II. Experimental Procedure

(1) Suspension Preparation and Consolidation

Dilute (8 vol% solids), dispersed (pH 3 using HNO_3). aqueous suspensions were prepared containing equal volumes of Ce–ZrO_2 and fine Al_2O_3, and varying Al_2O_3-platelet contents of 5.0, 12.5, and 20.0 vol% of the total solids (Table I). The

David J. Green—contributing editor

Manuscript No. 192016. Received February 19, 1996; approved July 5, 1996.
Supported by the National Science Foundation under Grant No. DMR-91-21948, and the Department of Basic Energy Science, the Midwest Superconductivity Consortium, Department of Energy under Grant No. DE-FFG02-90ER45427.
*Member, American Ceramic Society.

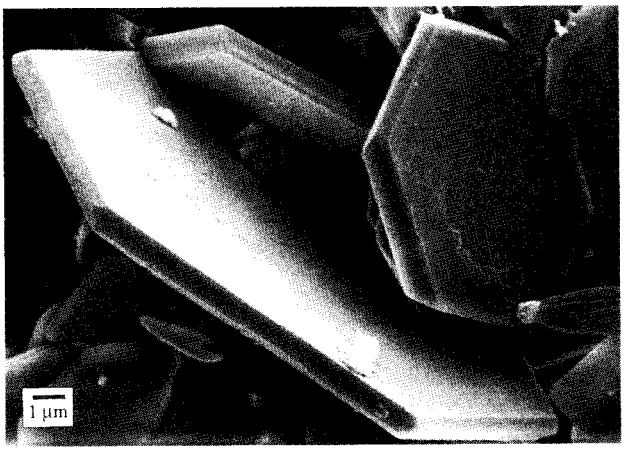

Fig. 1. SEM micrograph of the hexagonal-shaped Al_2O_3 platelets of basal orientation.

hexagonal-shaped Al_2O_3 platelets of basal orientation are shown in Fig. I. Each of the three ternary $Ce–ZrO_2/Al_2O_3/Al_2O_3$-platelet suspensions was centrifugally consolidated in polyethylene tubes placed within the swinging buckets of a centrifuge (model CL. Damon/IEC, Needham Hts., MA). Prior to consolidation. 4.0 mL of deionized water at pH 3 (using HNO_3) was placed in each of the four tubes. The suspensions were consolidated by consecutively centrifuging 40 separate suspension additions (in each tube) of 0.25 mL at ~2150 *g* for 2 min per addition. The pre-added water facilitated packing of layers of uniform thickness and provided long distances for particle displacement (and segregation) during consolidation. The consolidation procedure required 1.5–2.0 h; therefore, care was taken to maintain the bulk suspension at pH 3 under constant mixing. At the completion of consolidation, the supernatants were poured off. yielding four tabular green bodies (for each suspension) within their molds. More detailed accounts of the suspension preparation and consolidation procedures are given elsewhere."[20]

(2) *Thermal Processing*

At the completion of consolidation, molds were left in ambient, room temperature conditions. After 8-12 h, the green bodies had sufficient strength and shrinkage to allow removal from the polyethylene tubes. Virtually all moisture was removed from the green bodies after oven drying for a minimum of 6 h at an intermediate temperature (~50°C) and another 20 h at ~ 100°C.

Dried green bodies were tired at 1200°C (400°C/h ramp) for 1 h. The light sintering provided sufficient strength for sectioning and resulted in minimal densification (relative densities increased only 2–3 percentage points for all specimens) for examining the near-green microstructure. Specimens were sectioned with a diamond saw into rectangular prisms (~1.3 X 0.8 X 0.35 cm), which were annealed at 1600°C (800°C/h ramp) for 1 min, I, 4, 8, 16. 32, and 64 h.

The density and dimensions of all specimens were measured after drying, bisquing, and annealing. The density of the dried green specimens was estimated from measured specimen masses and dimensions. Once sintered, the density was measured using Archimedes principle. Measured dimensions were also used to calculate linear and volume shrinkages.

(3) *Sample Preparation and Microscopy*

Microscopy specimens for each anneal time were prepared by manual polishing, with 45, 30, and 15 μm diamond paste on glass (5 min each), followed by automatic polishing with 6 μm (1 h). 3 μm (0.5 h), 1 μm (3 h). and 0.25 μm (1 2 h) diamond paste on Texmet (Buehler. Lake Bluff, IL) polishing cloths. All specimens were thermally etched in air for 6 min at 1550°C and sputter coated with platinum. The microstructure was examined and photographed (1st row in Figs. 2–4) using a scanning electron microscope (JEOL JSM-35CF, Tokyo, Japan).

(4) *Image Processing and Feature Analysis*

SEM negatives of single layers. or equivalent area in the nonsegregated (20 vol% platelet) composites, were entered into a commercially available image analysis system (integrated microanalyzer for imaging and X-ray (IMIX), Princeton Gamma-Tech, Inc., Princeton, NJ) using a high-resolution video camera and light stage. Digitized images were 480 by 640 pixels with a range of 246 gray-scale intensities. Since binary images are required to distinguish microstructural features, the digitized gray-scale images were converted to binary images. Binary images were created for each anneal time of each composite to feature pores, Al_2O_3, and Al_2O_3 platelets. corresponding in Figs. 2–4 to the 2nd. 3rd. and 4th rows. respectively. Enhanced pore images were created by isolating all visible pores, utilizing charging contrast around pore edges in SEM images. However, the extent of charging prevented generation of suitable porosity images for the more porous 1 min anneal times. The lack of mutual solubility of Al_2O_3 and $Ce–ZrO_2$ and the absence of any intermediate phases precludes any significant changes in overall phase content during heat treatment. Therefore. the enhanced Al_2O_3 images were calibrated by adjusting the area fraction of Al_2O_3 in one layer (or representative area) to match the amount known to be present (calculated considering the sample porosity and Al_2O_3 fraction in the suspension). Finally, the enhanced Al_2O_3-platelet images were created by isolating all visible platelets from the Al_2O_3 images. Thus, all computer-enhanced images were created systematically, allowing comparison between different anneal times.

The Princeton Gamma-Tech software provided valuable geometrical data for each enhanced feature in binary images, allowing a quantitative description of the microstructural evolution. For both pores and platelets, this description includes changes in the feature volume fraction, dimensional anisotropy, and distribution across gradient layers. Feature volume fractions were determined by measuring the area fraction within regions of one layer thickness (or equivalent area). Quantification of dimensional anisotropy was made possible by measuring feature dimensions projected on the *x*- and F-axes (see Fig. 5), called "ferets."[24] Throughout this paper, the \--axis will always refer to the directions within the macroscopic planes of layers of aligned platelets. and the y-axis to the direction perpendicular. Phase distributions in gradient layers were obtained by measuring feature area (or area fraction) in 20 narrow boxes placed successively across a layer. The boxes typically spanned 15-18 pixels or ~2.5 μm of the gradient and sampled the entire width of the micrograph.

Table I. Starting Powders and Data

Powder	Percent of solids in suspensions (vol%) #1	#2	#3	Density (p/cm³)	Average particle size (μm)	Trade name. supplier
Al_2O_3 platelets	5.0	12.5	20.0	3.98"	1–25*,†	Elf Atochem. Paris, France
Fine Al_2O_3	47.5	43.8	40.0	3.98*	0.2*,‡	AKP-SO: Sumitomo Chemical. New York
Fractionated $Ce–ZrO_2$	47.5	43.8	40.0	6.20*	2.6‡	TZ-12Ce; Tosoh Ceramics Div., New Milford, CT

*From manufacturers' data. Measured using a Coulter LS130 (with fluid module) particle size analyzer.

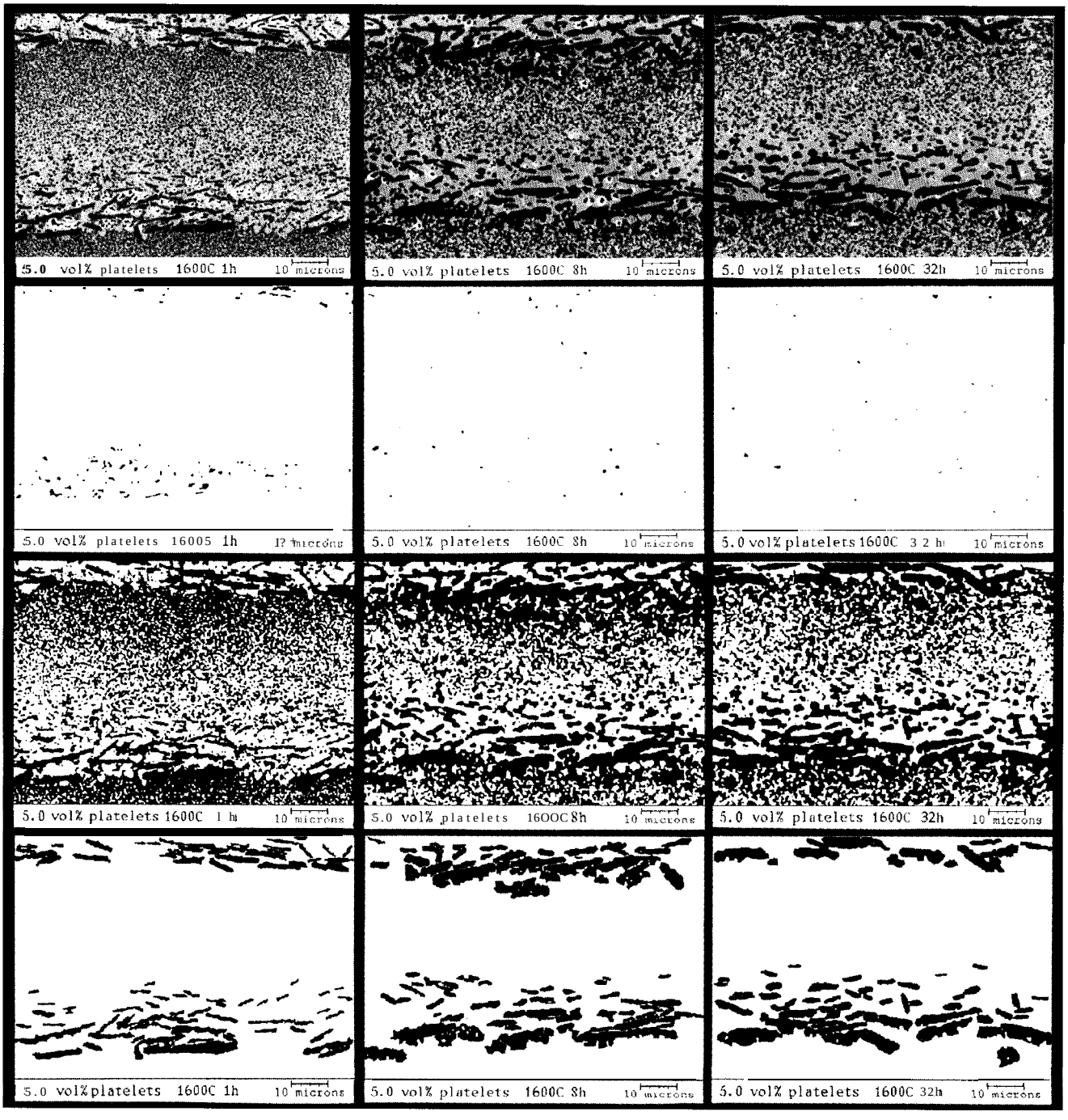

Fig. 2. SEM micrographs (1st row) of 5.0 vol% platelet FGL single layers at selected anneal times (1, 8, and 32 h) with corresponding binary images showing enhanced (black) porosity (2nd row), Al_2O_3 (3rd row), and Al_2O_3 platelets (4th row).

III. Results and Discussion

(1) Consolidation Behavior

The consolidation behavior of each suspension is revealed in Figs. 2-4 by examining the microstructures after the 1 h anneal time. In the 5.0 and 12.5 vol% suspensions, the combination of large centrifugal forces and a dispersed. low solids content suspension promoted segregation of suspension components by density and size (see Table I). The large Al_2O_3 platelets were the first to settle out of suspension additions, followed by the more dense, but much smaller, Ce–ZrO_2 particles and finally the fine Al_2O_3. On the contrary, the 20.0 vol% platelet suspension did not segregate; thus. constituents were uniformly distributed throughout each layer such that separate layers were not observable. This unexpected result and a proposed explanation are the subjects of another paper.“’

High particle packing densities were achieved in all composites despite the presence of anisometric platelets. As expected, relative green densities increased with decreasing platelet contents, as shown in Fig. 6. The key to attaining high particle packing densities lies in efficient particle packing via platelet alignment. Several factors contributed to efficient particle packing: large centrifugal forces on particles, repulsive interparticle forces, low solids content, multimodal packing, and segregation. Segregation provided constantly varying bimodal packing across gradient layers due to the density difference between Al_2O_3 and Ce–ZrO_2. Also, platelets segregated from the rest of the suspension could pack on top of one another in a “brick wall” fashion. These considerations could contribute to the significant difference in packing density between the segregated (5.0 and 12.5 vol% platelets) and nonsegregated (20.0 vol%) composites.

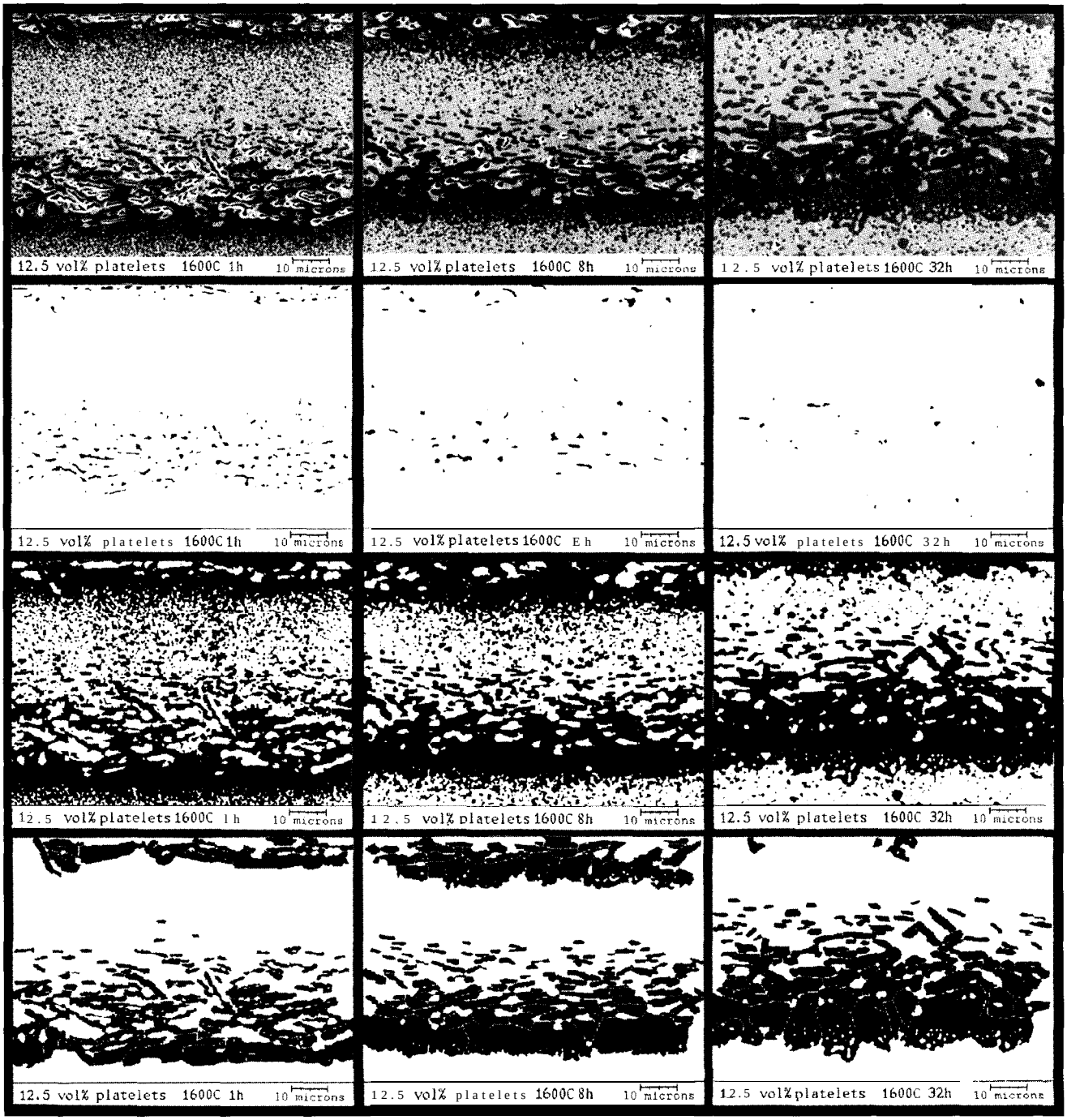

Fig. 3. SEM micrographs (1st row) of 12.5 vol% platelet FGL single layers at selected anneal times (1, 8, and 32 h) with corresponding binary images showing enhanced (black) porosity (2nd row). Al_2O_3 (3rd row). and Al_2O_3 platelet\ (4th row).

Cracking and delamination have been the largest factors inhibiting development of multilayer ceramic composites, due to the differential shrinkages of different phases during drying and sintering. Delamination is prevented within gradient layers because differential stresses are spread out over the gradient rather than concentrated at an interface. Delamination is also prevented between separate gradient layers. The ability of the large or dense particles of a new layer to consolidate freely and rapidly under high g-loads causes them to slightly penetrate the last particles consolidated in the previous layer. Thus, a sharper gradient is also formed between gradient layers.

(2) ***Densification, Shrinkage, and Pore Evolution***

Densification of the composites with increasing anneal time is displayed pictorially by enhanced pore images (Figs. 2-4, 2nd row) and quantitatively by plots of the pore fraction (Fig. 7). Several results were pertinent regardless of platelet content and phase distribution. High sintered densities (Fig. 7) were achieved despite the presence of matrix-constraining platelets and the use of pressureless sintering. Maximum relative sintered densities were 99.5%, 97.9%, and 97.1% for the 5.0. 12.5, and 20.0 vol% platelet composites, respectively. This result is explained by examining the linear shrinkage ratios (the ratio of the macroscopic linear shrinkages perpendicular and parallel to platelets) shown in Fig. 8. Increasing contents of aligned platelets limited constraint to directions within the plane of platelets, such that densification occurred primarily perpendicular to layers and platelets. Thus, platelet alignment caused anisotropic densification.

Evolution of the pore gradient in functionally gradient laminates (FGLs) with anneal time is shown pictorially by enhanced pore images (Figs. 2 and 3, 2nd row) and quantitatively by plots

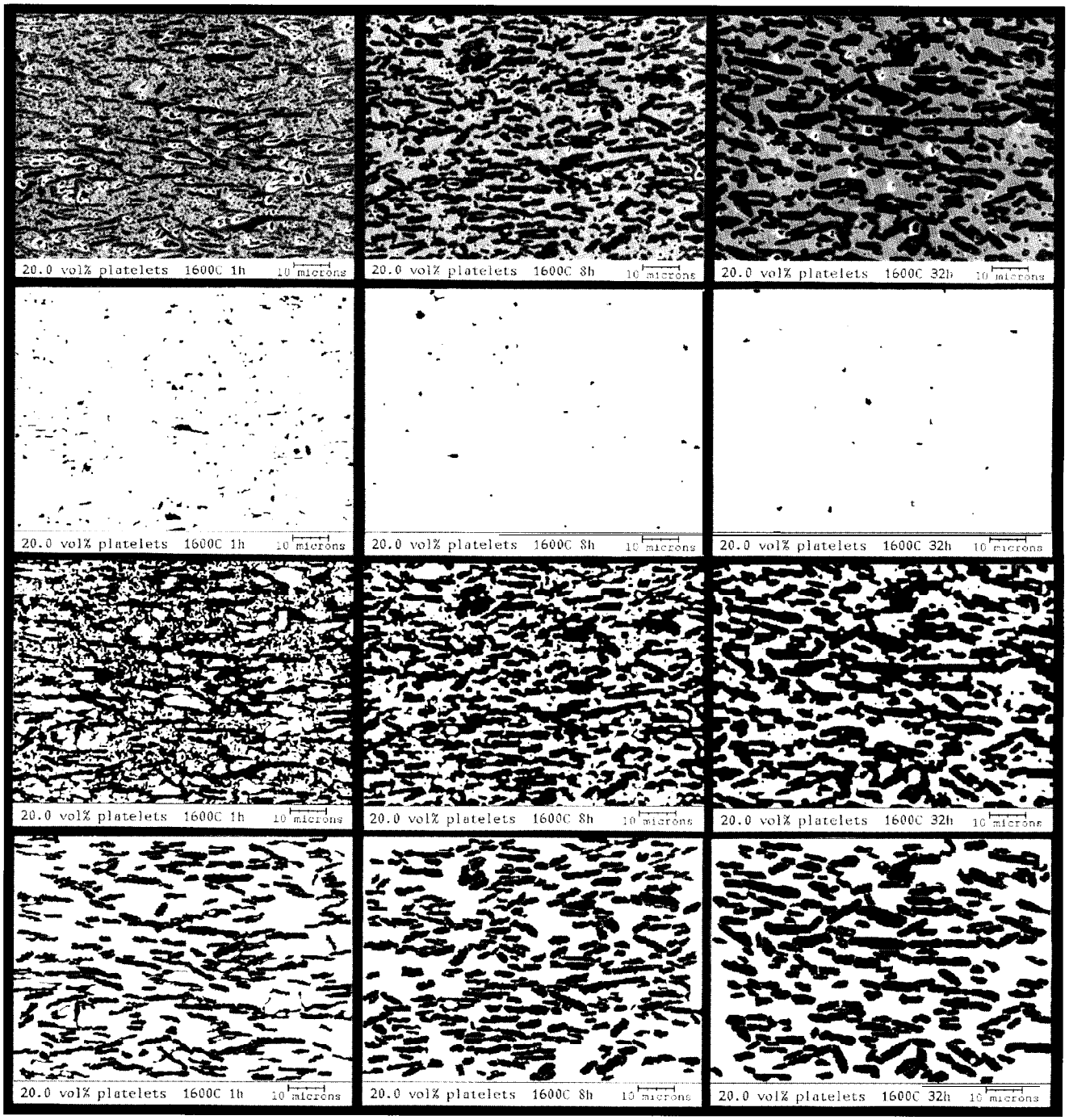

Fig. 4. SEM micrographs (1st row) of 20.0 vol% platelet composites at selected anneal times (1 8, and 32 h) with corresponding binary images showing enhanced (black) porosity (2nd row), Al_2O_3 (3rd row), and Al_2O_3 platelet\ (4th row).

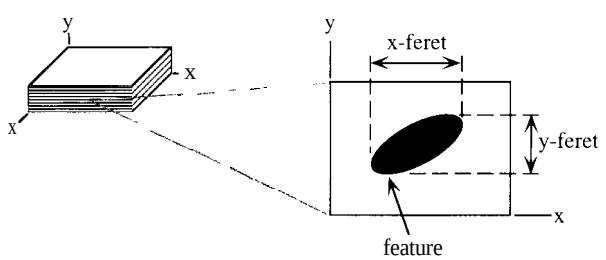

Fig. 5. Schematic defining measurement of x- and y-ferets of features.

of the pore distribution across a layer (Fig. 9). At short (up to 4 h) anneal times, pores are concentrated in platelet-containing regions. resulting from less efficient particle packing in these regions. These pores are also primarily located between the basal faces of platelets. occurring where two platelets stacked with a few smaller particles, or the edge of another platelet, sandwiched between them. Accordingly. the ratio of pore dimensions projected on the x- and y-axes (essentially an aspect ratio relegated to the directions of-interest) reveal that the oriented platelets induced a preferred orientation in pores at short anneal times (Fig. IO). At longer anneal times. the pore concentration in platelet regions and the dimensional anisotropy of pores both decreased. virtually disappearing by 32 and 16 h, respectively (Figs. 9 and IO). Although the data in Fig. IO is insufficient to draw strong conclusions, the initial preferred orientation of pores and decreasing dimensional anisotropy

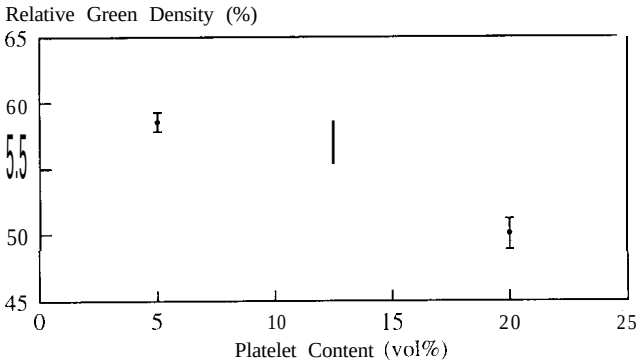

Fig. 6. Average relative green densities for 5.0. 12.5, and 20.0 vol% platelet composites. Error bars span the first standard deviation

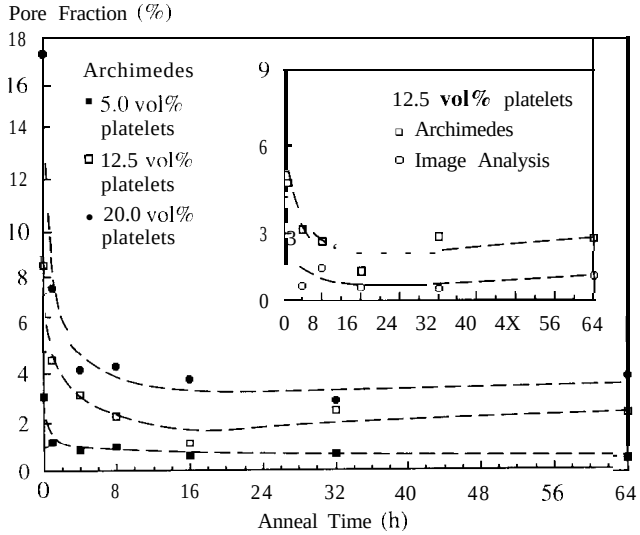

Fig. 7. Porosity evolution with anneal time in 5.0. 12.5. and 20.0 vol% platelet composites. showing changes in total pore fraction. Inset compares image analysis with Archimedes' porosity measurement for 12.5 vol% platelet composites.

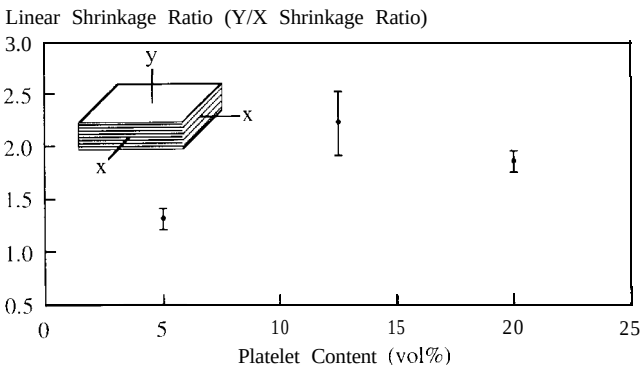

Fig. 8. Average linear shrinkage ratios for 5.0. 12.5, and 20.0 vol% platelet composites, showing the degree of densitication anisotropy. Error bars span one standard deviation.

with densification can be readily envisioned, as shown schematically in Fig. IO.

Additionally, data from image analysis suggest that at longer anneal times (over 4 h) a small fraction of pores appear and grow in the non-platelet-containing regions of layers, where essentially no pores were initially resolvable at short anneal times (Figs. 2 and 3, 2nd row, and Fig. 9). Comparison of the pore fractions measured using Archimedes' principle and image analysis (area fraction of single layers assumed equal to that of the FGL) reveal that image analysis consistently underestimated the pore fraction (Fig. 7). Thus, pores too small to be resolved at the magnifications necessary for image analysis of entire layers grew into larger, resolvable pores.

Possible mechanisms for the apparent pore growth in non-platelet-containing regions include constrained densification and pore coalescence during grain growth.[25,31] Constraint due to the aligned platelets would induce a relative tension in the non-platelet-containing regions of FGLs. Thus. grain growth in these regions could lead to pore coalescence where larger, more stable (higher coordination number) pores were formed.

The mechanism responsible for the large densifications observed in the platelet-containing regions can be explained in similar terms. Most pores bounded by platelets were initially large (on the order of the platelet size), but had low coordination numbers due to the effectively two-dimensional microstructure. These pores were unstable. and they readily densified. Moreover, stable pores were able to coalesce under the large platelet-induced grain growths. recoordinating into unstable pores. Pore coalescence has been demonstrated to occur when grain growth is faster than pore Shrinkage." Thus. the importance of grain growth in the densification behavior of the composites is evident.

(3) *Al_2O_3-Platelet Growth*

Platelet growth with increasing anneal time is displayed pictorially by enhanced platelet images (Figs. 2–4, 4th row). Al_2O_3 and Ce–ZrO_2 are mutually insoluble and exhibit no intermediate phases: therefore, increasing platelet area fraction with annealing (Fig. 11) is evidence that the large platelets grew at the expense of the finer Al_2O_3 particles. Since the platelets were initially aligned, the volume of the crystallographically oriented reinforcement phase increased dramatically via a platelet "seeded" growth. Shown in Fig. 11, the 5.0 vol% platelet FGL grew to ~18 vol%, and the 12.5 and 20.0 vol% platelet composites grew to ~50 vol% reinforcements. Implications for making higher platelet content composites consisting of larger platelets, without having to consolidate high contents of large platelets, could be significant.

The Al_2O_3 platelets preferentially grew perpendicular to the FGL layers on platelet basal planes, in contrast to familiar preferred growth in Al_2O_3. By themselves, the Al_2O_3 platelets prefer to grow in the directions of prismatic planes" producing more lower energy basal surface, as evidenced by the hexagonal shape (Fig. 1). Furthermore, a microstructural constraint argument would suggest that densitication and grain growth are greatest at the ends of a platelet, where the local microstructure undergoes a compressive strain.'" [30]

The measured anisotropic platelet growth (Fig. 12) is a result of several factors. In FGLs, many platelets are initially in direct contact with the fine Al_2O_3 particles of the previous layer, providing a large source of consumable grains, with many diffusion paths (grain boundaries)," and few second-phase grains (Ce–ZrO_2) to hinder grain growth." Microstructural constraint also contributes to platelet growth anisotropy."' [30] Since platelets generally lie end-to-end. there is little room for growth to occur before platelets laterally impinge on one another. Consequently, the less-constrained densitication perpendicular to layers and platelets is faster, reaching the grain growth regime earlier during sintering. Despite having a wider grain size distribution (more platelets),"' the homogeneous 20.0 vol% platelet samples had less platelet growth and less anisotropic growth than would be expected relative to the layered 12.5 vol% platelet samples. The differences in the microstructure designs facilitated more growth and growth anisotropy in the 12.5 vol% platelet samples because of increased constraint anisotropy and availability of consumable fine Al_2O_3 grains. Thus, platelet alignment and microstructural design can be used to initiate and control anisotropic grain growth, even in orientations typically less favored.

Microstructural evidence of the platelet "seeded" growth is found in composites annealed for short times. Figure 13(a)

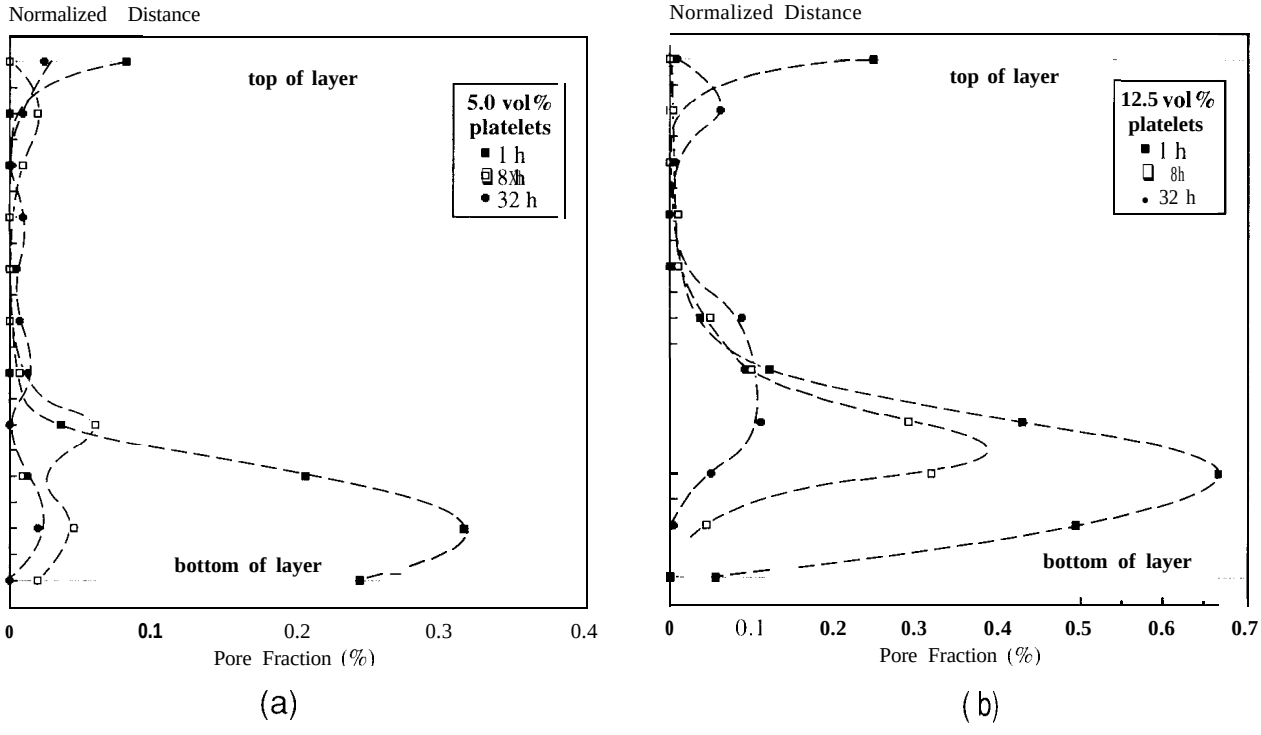

Fig. 9. **Porosity evolution** with anneal time in (a) 5.0 and (b) 12.5 vol% platelet FGLs showing changes in the pore fraction across a single layer.

shows platelets growing into the fine Al_2O_3 of the previous layer in the 12.5 vol% platelet FGL. The growth of platelets into the line Al_2O_3 grains was mostly nonfaceted. although many platelets maintained the basal facet during growth, as shown in Fig. 13(b). Notice the visible outline of the original ~1 μm thick platelet "seed" at the top of the largest grain shown. The ability of a growing platelet to maintain the basal facet was dependent on local grain boundary misorientations[32] and the presence and size of neighboring Ce–ZrO_2 grains. The presence of a liquid phase (due to impurities) at grain boundaries would also promote basal faceting.[32,34] However, it is unlikely that a sufficient amount of impurities to form a liquid phase was present, considering the purity of starting powders and processing techniques used. Furthermore. since liquid phases prefer to wet the basal plane. greater decreases in basal plane growth are usually observed with a liquid phase present.[34]

The extreme grain growth that occurs after longer anneal times is shown in Fig. 13(c), where the large-platelet-seeded Al_2O_3 grains completely encompass Ce–ZrO_2 grains, and Ce–ZrO_2 grains engulf unconsumed fine Al_2O_3 grains.[33,35,36] In order to reach this state, grain growth must continue even after platelet seeds are no longer in direct contact with tine Al_2O_3 grains. A large driving force must exist for such extreme grain

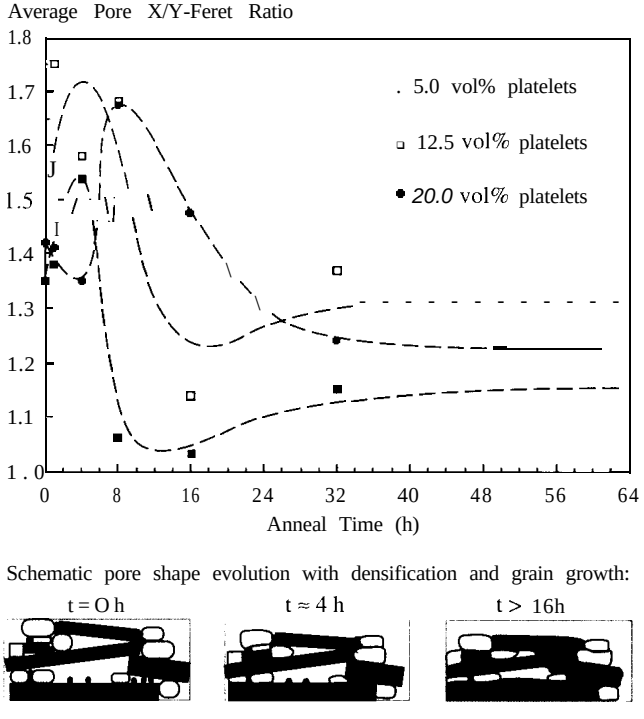

Fig. 10. Porosity evolution with anneal time in 5.0, 12.5, and 20.0 vol% platelet composites showing changes in the ratio of pore dimensions projected on the *x*- and *y*-axes and corresponding schematic representation.

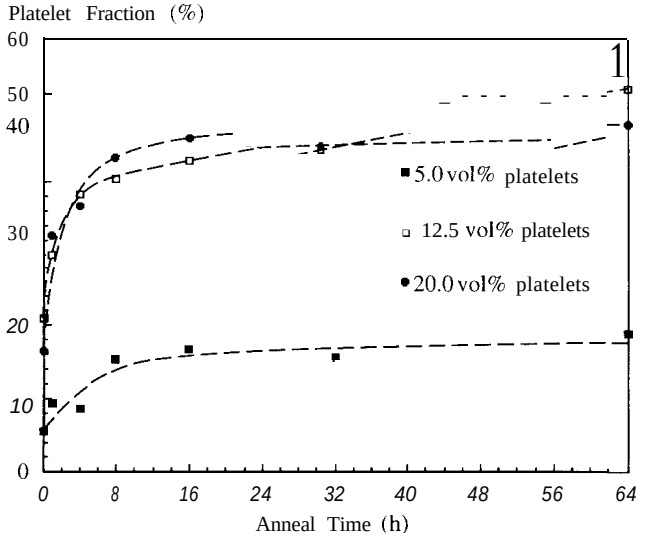

Fig. 11. Al_2O_3-platelet evolution with anneal time in 5.0, 12.5, and 20.0 vol% platelet composites showing changes in the platelet volume fraction.

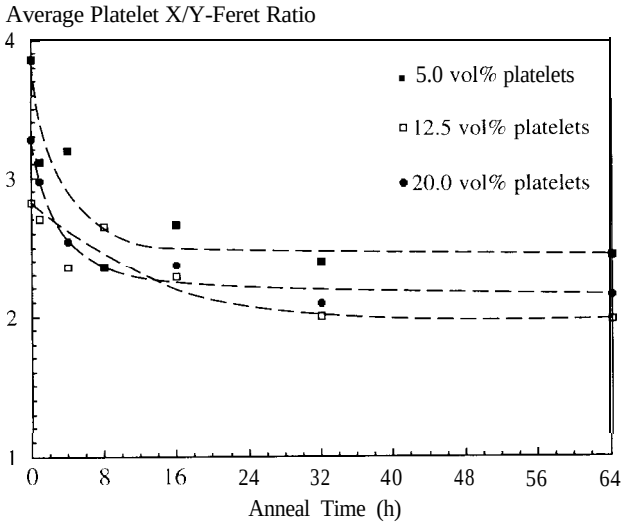

Fig. 12. Al_2O_3-platelet evolution with anneal time in 5.0, 12.5, and 20.0 vol% platelet composites showing changes in the ratio of platelet dimensions projected on the *x*- and *y*-axes.

growth to occur. The source of this driving force is examined by considering the phase gradient evolution with anneal time.

(4) Phase Redistribution via Grain Growth

Evolution of the phase gradient in FGLs with anneal time is shown pictorially by enhanced Al_2O_3 images (Figs. 2 and 3, 3rd row) and quantitatively by plots of the Al_2O_3 area fraction distribution across gradient layers (Fig. 14). As the anneal time is increased. the Al_2O_3 fraction increases in the platelet-containing region and decreases in the gradient regions that initially had larger contents of tine Al_2O_3. Thereby, platelet growth corresponds to a migration of Al_2O_3 across the layer gradients to platelets. resulting in phase segregation. Recall that gradients exist not only within each layer but. more significantly, a sharper gradient also exists between separate layers.

The phase redistribution is presumably **due to** the large grain size gradient across gradient layers. Phase and curvature gradients can both contribute to the chemical potential gradient that drives diffusion. Since Al_2O_3 and $Ce–ZrO_2$ are virtually immiscible and exhibit no intermediate phases. bulk two-phase equilibrium eliminate\ a bulk chemical potential gradient. On the other hand. curvature-induced chemical potential gradients do exist. due to the large grain sire gradients within and between gradient layers. Diffusion driven by the grain size gradient results in preferential growth of larger. lower energy grains at the expense of smaller. higher energy grains. The grain growth occurs by either Ostwald ripening or coalescence processes. Coalescence requires that grain\ of the same phase come into

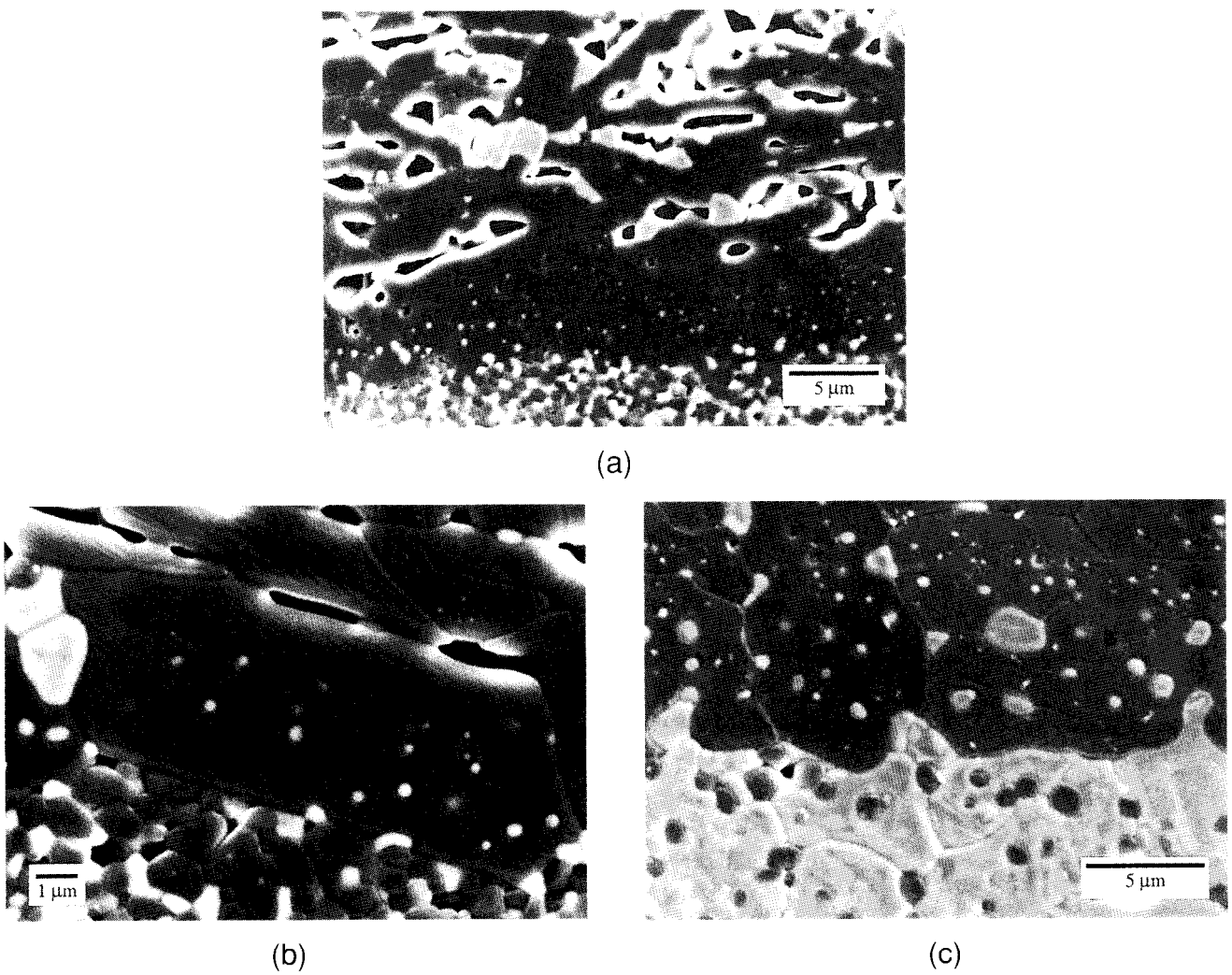

Fig. 13. SEM micrographs of the inter-layer region in 12.5 vol% platelet composites after annealing for (a) and (b) 1 h and (c) 64 h, showing platelet-seeded growth.

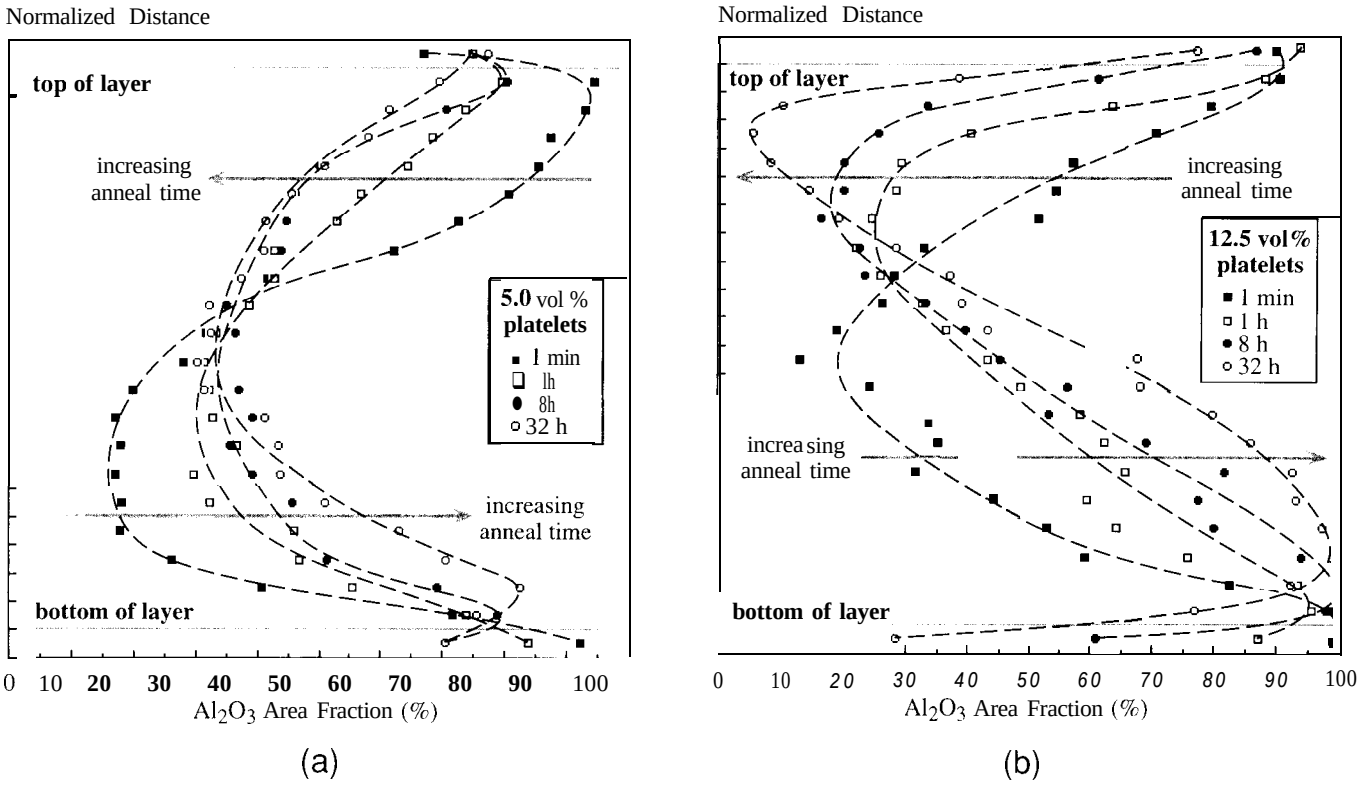

Fig. 14. Gradient evolution with anneal time in (a) 5.0 and (b) 12.5 vol% platelet FGLs showing changes in Al_2O_3 concentration across a single layer.

contact through grain boundary movement. whereas Ostwald ripening requires no direct contact.

The intergranular Ce–ZrO_2 grains generally grew by coalescence until they either (1) were engulfed by growing Al_2O_3 platelets. becoming intragranular. or (2) grew abnormally at a critical grain size and fraction of neighboring Al_2O_3 grains. Lange and Hirlinger also observed growth by coalescence. followed by abnormal grain growth after a critical fraction of inclusion grains or relative size of matrix grains was reached. Their studies were for homogeneous composites of Al_2O_3 matrix grains with ZrO_2 inclusions," and vice versa.[35] Microstructural observations contained in both previous studies are similarly shown in Fig. 13(c). Also. the fractions of either Al_2O_3 or Ce–ZrO_2 inclusions present (Fig. 14) in locations where abnormal grain growth occurred appears to support the previous work.

The Al_2O_3 platelets initially grew by coalescence. consuming tine Al_2O_3 grains until they were no longer in direct contact. At later stages. the Al_2O_3 platelets continued to grow by an Ostwald ripening (coarsening) process because of their large grain boundary energy anisotropy, and they were too large and separated from tine grains to take part in intergranular grain boundary movement necessary for coalescence. As described by the Gibbs-Thomson equation. the driving force for grain coarsening is the difference in chemical potential due to a difference in mean surface curvature at two locations, either on the same grain or different grains of the same phase. The basal plane of a growing platelet essentially has zero curvature, hence the large driving force for consuming much smaller grains of the same phase.

The observation that the Ce–ZrO_2 fraction engulfed by growing Al_2O_3 platelets is lower than the fraction initially present (Figs. 13 and 14) supports the mechanism of Ostwald ripening for Al_2O_3-platelet growth. Although platelets could initially coalesce with neighboring tine Al_2O_3 grains, the buildup of Ce–ZrO_2 grains at the interface would quickly require that either many Ce–ZrO_2 grains become intragranular or platelet growth continue by Ostwald ripening. Analysis of the effective diffusion fluxes as a function of position in the gradient could lend further insight into the driving forces behind the phase segregation observed in FGLs.

Another interesting feature of Fig. 15 is the intersection of Al_2O_3 fraction curves at a specific position in the gradient, where there is no effective Al_2O_3 redistribution. The intersection could be pointing to the best second-phase (Ce–ZrO_2 in this case) content and grain size for preventing matrix (Al_2O_3 in this case) grain growth. Gradient microstructures could be used to determine optimal microstructural characteristics for either preventing or enhancing grain growth in uniform composites.

IV. Summary

In the present study of microstructure development in Al_2O_3-platelet-reinforced Ce–ZrO_2/Al_2O_3 composites. image analysis successfully elucidated important aspects of microstructure development. providing valuable quantitative and visual information High green and sintered densities were achieved despite the presence of large, highly anisometric. matrix-constraining platelets. Platelet alignment facilitated efficient particle packing and resulted in anisotropic shrinkage and densification. Constraint that typically inhibits densification during pressureless sintering of platelet-containing composites was limited to two dimensions, allowing less-constrained densification to occur perpendicular to layers and aligned platelets. Porosity measurement by image analysis was highly resolution dependent, leading to underestimated pore fractions. At short anneal times, pores were predominantly located between platelets and exhibited dimensional anisotropy induced by the oriented platelets. Pores surrounded by platelets were unstable, having a low coordination number due to the effectively two-dimensional microstructure, and readily densified. Pores in non-platelet-containing regions of FGLs were apparently able to coalesce into larger, stable pores during grain growth. Al_2O_3 platelets grew at the expense of smaller particles of the same phase, substantially increasing the volume and size of the oriented reinforcements. Al_2O_3-platelet growth was anisotropic, favoring

growth on lower energy basal planes, despite typically preferred growth on higher energy prismatic planes. The anisotropic growth was a result of microstructure design and constraint. In FGLs, platelet growth corresponded to a migration of' Al_2O_3 across the gradient layer and phase segregation, driven by the large grain size gradient. The Al_2O_3 platelets initially grew by coalescence. consuming tine Al_2O_3 grains. However. the buildup of Ce–ZrO_2 grains at the interface and the observed phase segregation over long heat treatments suggest that Ostwald ripening also contributed to platelet growth, especially during the later stages.

Acknowledgments: The authors thank J. Blendell (NIST) for providing the Atochem 41.0. platelets and E. B. Slamovich for valuable comments regarding the manuscript.

References

[1]K. Heussner and N. Claussen, "Yttria- and Ceria-Stabilized Tetragonal Zirconia Polycrystals (Y-TZP, CE-TZP) Reinforced with Al_2O_3 Platelets," *J. Eur. Ceram. Soc.*, **5**, 193–200 (1989).

[2]Y. Chou and D. J. Green, "Silicon Carbide Platelet/Alumina Composites: II. Mechanical Properties," *J. Am. Ceram. Soc.*, **76** [6] 1452–58 (1983).

[3]Y. Chou and D. J. Green, "Silicon Carbide Platelet/Alumina Composites: III. Toughening Mechanisms," *J. Am. Ceram. Soc.*, **76** [8] 1985–92 (1993).

[4]F. J. Lee, M. S. Sandlin, and K. J. Bowman, "Toughness Anisotropy in Textured Ceramic Composites," *J. Am. Ceram. Soc.*, **76** [7] 1793–800 (1993).

[5]X. Huang and P. S. Nicholson, "Mechanical Properties and Fracture Toughness of α-Al_2O_3-Platelet-Reinforced Y-PSZ Composites at Room and High Temperatures," *J. Am. Ceram. Soc.*, **76** [5] 1294–301 (1993).

[6]I. K. Cherian and W. M. Kriven, "Fabrication by Colloidal Filtration of Alumina Platelet Reinforced 3Y-TZP: Mechanical Properties"; pp. 387–98 in Ceramic Transactions, Vol. 46, *Advances in Ceramic-Matrix Composites II*. American Ceramic Society, Westerville, OH, 1994.

[7]K. J. Bowman, "Textures in Ceramic Materials"; in Proceedings of the 10th International Conference on Textures of Materials (ICOTOM), *Mater. Sci. Forum*, **156–57**, 43–56 (1994).

[8]T. Claassen and N. Claussen, "Processing of Ceramic-Matrix/Platelet Composites by Tape Casting and Lamination," *J. Eur. Ceram. Soc.*, **10**, 263–71 (1992).

[9]M. Belmonte, R. Moreno, J. S. Moya, and P. Miranzo, "Obtention of Highly Dispersed Platelet-Reinforced Al_2O_3 Composites," *J. Mater. Res.*, **29**, 179–83 (1994).

[10]M. S. Sandlin and K. J. Bowman, "Textures in AlN–SiC Composite Ceramics"; pp. 263–68 in *Covalent Ceramics II: Non-Oxides* (*Mater. Res. Soc. Symp. Proc.*, Vol. 327). Edited by A. R. Baron et al. Materials Research Society, Pittsburgh, PA, 1994.

[11]M. S. Sandlin, J. E. Root, and K. J. Bowman, "Texture in SiC-Seeded AlN," *Acta Mater.*, in press.

[12]R. K. Roeder, K. J. Bowman, and K. P. Trumble, "Texture and Microstructure Development in Al_2O_3-Platelet Reinforced Ce–ZrO_2/Al_2O_3 Laminates Produced by Centrifugal Consolidation," *Textures Microstruct.*, **24**, 43–52 (1995).

[13]F. F. Lange, "Forming a Ceramic by Flocculation and Centrifugal Casting," U.S. Pat. No. 4 624 808, Nov. 25, 1986.

[14]F. F. Lange and K. T. Miller, "A Colloidal Method to Ensure Phase Homogeneity in β″-Al_2O_3/ZrO_2 Composite Systems," *J. Am. Ceram. Soc.*, **70** [12] 896–900 (1987).

[15]F. F. Lange, "Powder Processing Science for Increased Reliability," *J. Am. Ceram. Soc.*, **72** [1] 3–15 (1989).

[16]F. F. Lange, " 'New' Interparticle Potential Paradigm for Advanced Powder Processing"; pp. 185–201 in Ceramic Transactions, Vol. 22, *Ceramic Powder Science IV*. Edited by S. Hirano, G. L. Messing, and H. Hausner. American Ceramic Society, Westerville, OH, 1991.

[17]B. V. Velamakanni and F. F. Lange, "Effect of Interparticle Potentials and Sedimentation on Particle Packing Density of Bimodal Particle Distribution during Pressure Filtration," *J. Am. Ceram. Soc.*, **74** [1] 166–72 (1991).

[18]J. C. Chang, B. V. Velamakanni, F. F. Lange, and D. S. Pearson, "Centrifugal Consolidation of Al_2O_3 and Al_2O_3/ZrO_2 Composite Slurries vs Interparticle Potentials: Particle Packing and Mass Segregation," *J. Am. Ceram. Soc.*, **74** [9] 2201–204 (1991).

[19]E. Beylier, R. L. Pober, and M. J. Cima, "Centrifugal Casting of Ceramic Components"; pp. 529–36 in Ceramic Transactions, Vol. 12, *Ceramic Powder Science III*. Edited by G. L. Messing, S. Hirano, and H. Hausner. American Ceramic Society, Westerville, OH, 1990.

[20]R. K. Roeder, G. A. Steinlage, K. J. Bowman, and K. P. Trumble, "Preventing Segregation during Centrifugal Consolidation of Particulate Suspensions," *J. Am. Ceram. Soc.*, **78** [9] 2367–73 (1995).

[21]G. Steinlage, R. Roeder, K. Trumble, K. Bowman, S. Li, and M. McElfresh, "Preferred Orientation of BSCCO via Centrifugal Slip Casting," *J. Mater. Res.*, **9** [4] 1–4 (1994).

[22]D. B. Marshall, J. J. Ratto, and F. F. Lange, "Enhanced Fracture Toughness in Layered Microcomposites of Ce-ZrO_2 and Al_2O_3," *J. Am. Ceram. Soc.*, **74** [12] 2979–87 (1991).

[23]J. S. Moya, A. J. Sanchez-Herencia, J. Requena, and R. Moreno, "Functionally Gradient Ceramics by Sequential Slip Casting," *Mater. Lett.*, **14**, 333–35 (1992).

[24]Princeton Gamma-Tech (PGT), Inc., *Integrated Microanalyzer for Imaging and X-ray (IMIX) Software Manual*, Version 7. Edited by M. L. Kuszewski. Princeton Gamma-Tech, Inc., Princeton, NJ, 1993.

[25]J. Zhao and M. P. Harmer, "Effect of Pore Distribution on Microstructural Development: II. First and Second Generation Pores," *J. Am. Ceram. Soc.*, **71** [7] 530–39 (1988).

[26]B. J. Kellet and F. F. Lange, "Thermodynamics of Densification: I. Sintering of Simple Particle Arrays, Equilibrium Configurations, Pore Stability, and Shrinkage," *J. Am. Ceram. Soc.*, **72** [5] 725–34 (1989).

[27]F. F. Lange and B. J. Kellet, "Thermodynamics of Densification: II. Grain Growth in Porous Compacts and Relation to Densification," *J. Am. Ceram. Soc.*, **72** [5] 735–41 (1989).

[28]E. B. Slamovich and F. F. Lange, "Densification of Large Pores: I. Experiments," *J. Am. Ceram. Soc.*, **75** [9] 2498–508 (1992).

[29]O. Sudre and F. F. Lange, "Effect of Inclusions on Densification: I. Microstructural Development in an Al_2O_3 Matrix Containing a High Volume Fraction of ZrO_2 Inclusions," *J. Am. Ceram. Soc.*, **75** [3] 519–24 (1992).

[30]O. Sudre, G. Bao, B. Fan, F. F. Lange, and A. G. Evans, "Effect of Inclusions on Densification: II. Numerical Model," *J. Am. Ceram. Soc.*, **75** [3] 525–31 (1992).

[31]O. Sudre and F. F. Lange, "The Effect of Inclusions on Densification: III. The Desintering Phenomenon," *J. Am. Ceram. Soc.*, **75** [12] 3241–51 (1992).

[32]J. Roedel and A. M. Glaeser, "Anisotropy of Grain Growth in Alumina," *J. Am. Ceram. Soc.*, **73** [11] 3292–301 (1990).

[33]F. F. Lange and M. M. Hirlinger, "Hindrance of Grain Growth in Al_2O_3 by ZrO_2 Inclusions," *J. Am. Ceram. Soc.*, **67** [3] 164–68 (1986).

[34]W. A. Kaysser, M. Sprissler, C. A. Handwerker, and J. E. Blendell, "Effect of a Liquid Phase on the Morphology of Grain Growth in Alumina," *J. Am. Ceram. Soc.*, **70** [5] 339–43 (1987).

[35]F. F. Lange and M. M. Hirlinger, "Grain Growth in Two-Phase Ceramics: Al_2O_3 Inclusions in ZrO_2," *J. Am. Ceram. Soc.*, **70** [11] 827–30 (1987).

[36]B. Kibbel and A. H. Heuer, "Exaggerated Grain Growth in ZrO_2-Toughened Al_2O_3," *J. Am. Ceram. Soc.*, **69** [3] 231–36 (1986).